

Topological Fracton Quantum Phase Transitions by Tuning Exact Tensor Network States


Guo-Yi Zhu^{1,*}, Ji-Yao Chen^{2,3,†}, Peng Ye^{2,4,‡} and Simon Trebst^{1,§}

¹*Institute for Theoretical Physics, University of Cologne, Zùlpicher StraÙe 77, 50937 Cologne, Germany*

²*Guangdong Provincial Key Laboratory of Magnetoelectric Physics and Devices, School of Physics, Sun Yat-sen University, Guangzhou, 510275, China*

³*Dahlem Center for Complex Quantum Systems, Freie Universitat Berlin, 14195 Berlin, Germany*

⁴*State Key Laboratory of Optoelectronic Materials and Technologies, Sun Yat-sen University, Guangzhou, 510275, China*

 (Received 9 March 2022; revised 6 March 2023; accepted 4 May 2023; published 25 May 2023)

Gapped fracton phases of matter generalize the concept of topological order and broaden our fundamental understanding of entanglement in quantum many-body systems. However, their analytical or numerical description beyond exactly solvable models remains a formidable challenge. Here we employ an exact 3D quantum tensor-network approach that allows us to study a \mathbb{Z}_N generalization of the prototypical X cube fracton model and its quantum phase transitions between distinct topological states via fully tractable wave function deformations. We map the (deformed) quantum states exactly to a combination of a classical lattice gauge theory and a plaquette clock model, and employ numerical techniques to calculate various entanglement order parameters. For the \mathbb{Z}_N model we find a family of (weakly) first-order fracton confinement transitions that in the limit of $N \rightarrow \infty$ converge to a continuous phase transition beyond the Landau-Ginzburg-Wilson paradigm. We also discover a line of 3D conformal quantum critical points (with critical magnetic flux loop fluctuations) which, in the $N \rightarrow \infty$ limit, appears to coexist with a gapless deconfined fracton state.

DOI: [10.1103/PhysRevLett.130.216704](https://doi.org/10.1103/PhysRevLett.130.216704)

Quantum states with intrinsic topological order distinguish themselves through long-range entanglement [1], quasiparticle excitations with exotic statistics [2], and their applicability as quantum memories [3]. Such states have been widely studied in two spatial dimensions (2D), e.g., as ground states of the toric code (TC) [3], which has also allowed for recent experimental realizations engineered in state-of-the-art quantum simulators [4,5]. Exploring such states in three-dimensional (3D) settings has given rise to the family of fracton topological orders [6–9] with strictly immobile excitations, the eponymous fractons, which have ignited interest not only in the fields of quantum information and quantum matter but also elasticity and gravity [10,11]. The simplest exactly solvable fracton model is the X cube (XC) [9] where the mobility constraint is deeply rooted in the absence of string operators [7]. The ground states of the XC span a degenerate manifold which is insensitive to local perturbations and whose peculiar subextensivity can be traced back to an intimate connection to 2D topological order via a coupled-layer-construction [12–19]. Like the TC which is equivalent to a \mathbb{Z}_2 lattice gauge theory [3], the XC can be viewed as a generalized lattice gauge theory coupled to \mathbb{Z}_2 matter with certain subsystem symmetries [9]; in the long wave-length limit, it is equivalent to an off-diagonal $U(1)$ tensor gauge theory that is turned massive via a Higgs mechanism [20–24] and where the matter charge has conserved higher moments [25–33].

Despite this impressive understanding of fracton physics, there are still a number of unresolved questions. One is the

principal nature of quantum phase transitions (QPTs) involving fracton topological phases, which due to their nonlocal structure have to go beyond the traditional Landau-Ginzburg-Wilson paradigm. Although there have been analytical attempts based on Hamiltonian duality, series expansions, or phenomenological field theories [13,34–40], a direct microscopic investigation, e.g., by considering deformations of exactly solvable Hamiltonians as for their 2D counterparts, has remained largely out of scope of current approaches.

Here we follow a different route and study wave function deformations that allow us to move from the exactly known ground states of certain fracton models through QPTs to topologically trivial states devoid of any fractons. Such paths differ from the conventional Hamiltonian deformations by spacetime anisotropy and could yield space-conformal quantum critical points [41]. In doing so, we employ tensor-network (TN) wave functions that allow us to exactly tune these quantum states along a chosen path—an approach previously employed in the context of 2D topological order [41–50]. For the 3D fracton order of interest here, we identify QPTs along the path by numerical TN calculations that are based on an analytical quantum-classical mapping and allow us to calculate various entanglement order parameters [44,45,48,51–55] as diagnostics. For the \mathbb{Z}_N generalized XC fracton model our main findings can be concentrated around a line of 3D space-conformal deconfined quantum critical points, where the deconfined fractons are connected by critical fluctuating

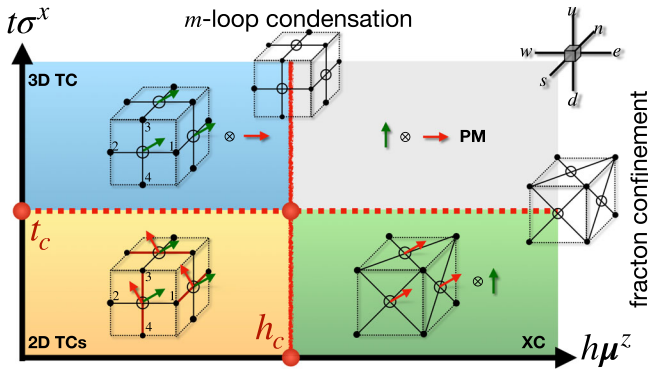


FIG. 1. Phase diagram of tuning the exact quantum TN state between the stacked 2D toric codes, 3D toric code, X cube, and the trivial paramagnet (PM) for \mathbb{Z}_N gauge group. The TN states are illustrated in dual cubes, where the black dots denote the virtual variables and the red (green) arrow denotes physical spin σ^z (μ^z), satisfying $\mu^z = \omega^{n_1 - n_2 - n_3 + n_4}$, $\sigma^z = \omega^{n_4 - n_3}$. The classical TNs lying at the QPTs show the wave function norm.

strings. In one direction, the string can either condense resulting in a gapped \mathbb{Z}_N fracton phase, or confine a pair of fractons into a fracton dipole thereby falling into the stacked 2D TCs phase; in the other direction, monopole proliferation leads to a complete fracton confinement in a weak first-order transition that turns continuous in the un-Higgsed $N \rightarrow \infty$ limit.

Parent wave function.—Our starting point is the observation that stacked intersecting 2D TCs can act as a parent for realizing both the XC and 3D TC models through condensing its elementary excitations—magnetic flux loops or monopoles [12,13,34,56]. In terms of wave functions, this motivates us to adopt the ground state of the stacked 2D TCs as a parent wave function and study its deformations that will pass through QPTs to either the XC or 3D TC ground states, as illustrated in Fig. 1. At the fixed point the wave function is a stack of dual 2D Ising quantum paramagnets [3]

$$|\psi_0\rangle = \sum_{\{s\}} |Z_{p \cap q} = s_p s_q\rangle, \quad (1)$$

where the Pauli z matrix Z for the physical spin on a link $l = p \cap q$ can be recast as the domain wall between classical Ising spins $s = \pm 1$ on the two adjacent plaquettes p, q in the same plane. On every link this results in two spins from two intersecting planes. Now let us rotate the local basis into $\mu_l^z \equiv Z_{l_1} Z_{l_2}$, $\mu_l^x \equiv X_{l_2}$, $\sigma_l^x \equiv X_{l_1} X_{l_2}$, $\sigma_l^z \equiv Z_{l_1}$, where l_1, l_2 lie in $xz(yx)(zy)$ and $xy(yz)(zx)$ planes, respectively (see Supplemental Material (SM) [57]). The ground state fulfills

$$\prod_{l \in \ast} \mu_l^z = 1, \quad \prod_{l \in \square} \sigma_l^x = 1 \quad (2)$$

for every vertex \ast and cube \square , respectively. These are the Gauss laws for the 3D vector and tensor gauge theories, respectively, which makes it natural to interpret the subsystem $\{\mu^z\}$ as the 3D TC [58], while $\{\sigma^x\}$ as the XC [9,20,21]. The parent state $|\psi_0\rangle$ is free of charge, while any violations of Eq. (2) define the boson (e) and fracton (f) charge excitations. The magnetic flux loop (m loop) is composed of a loop of m particles that penetrate plaquettes with $\prod_{l \in \square} \mu_l^x = -1$ [58], while the magnetic monopole is defined on the site satisfying $\prod_{l \in \ast} \sigma_l^z = -1$ for inplane vertices + [9]. Notice that the monopoles in the XC subsystem are entangled with the proliferating electric string turning points of the TC subsystem. Thus if either one subsystem is traced out, one would get a mixed state with m loops or monopole excitations [57].

To explore the QPTs induced by condensing these elementary excitations, we add fluctuations of the m loop and monopoles by a local nonunitary deformation [59]

$$|\psi(t, h)\rangle = \exp\left(\frac{1}{2} \sum_l h \mu_l^z + t \sigma_l^x\right) |\psi_0\rangle. \quad (3)$$

Here $h \mu^z$ fluctuates m loops and adds electric string tension to confine the boson charge, distilling the XC state from $|\psi_0\rangle$, which in the $h \rightarrow \infty, t = 0$ limit turns into the exactly solvable XC TN state as a cuboid condensate [57,61,62]. $t \sigma^x$ fluctuates the monopole (lineon) and turns on electric membrane tension to confine the fracton, distilling the 3D TC out of $|\psi_0\rangle$ as a loop condensate. Such deformations can be captured by an exact, frustration-free Rokhsar-Kivelson Hamiltonian, which in the perturbative limit is equivalent to turning on magnetic fields along μ^z and σ^x [57]. In our numerical analysis, we express the state (3) as a 3D projected entangled paired state (PEPS) with finite bond dimension (see Fig. 1).

Quantum classical correspondence.—The TN wave functions (3) can be mapped onto effectively classical models by defining $\langle \psi | \psi \rangle$ as a partition function [41,48,60,63] over the ensemble of the virtual TN variables. We find analytically that this partition function factorizes into

$$\langle \psi | \psi \rangle = \sum_{\{s\}} e^{-\epsilon_g} \times \sum_{\{\tau\}} e^{-\epsilon_p}, \quad (4)$$

where the two terms

$$\epsilon_g = -h \sum_{\square} s \begin{array}{c} \square \\ \hline \square \end{array} s, \quad \epsilon_p = -t \sum_{\square} \begin{array}{c} \tau \\ \hline \tau \end{array} \tau \quad (5)$$

are precisely the cubic lattice variants of the classical \mathbb{Z}_2 gauge [64] and plaquette [65–67] models, describing the (fluctuating) loop gas and fracton matter, respectively. Here s creates the m particle [48], while τ measures the fractons in the dual lattice [57]. For the latter, the parameter

TABLE I. Quantum classical correspondence between wave function and statistical model.

Quantum toric code	Tensor network	Classical gauge
μ^z	Z_\square	W_\square
$\langle e e\rangle$	X_\square	't Hooft string
$\langle \psi \prod_{p \in \partial M} m_p \rangle$	$\prod_{\square \in M} Z_\square$	Wilson loop
Quantum fracton	Tensor network	Classical plaquette
Quadrupole	Z_\square	W'_\square
$\langle \psi \text{monopole} \rangle$	X_\square	Twist defect
$\ \prod_{j \in \partial \partial M} f_j \ ^2$	$\prod_{\square \in M} Z_\square$	$\prod_{j \in \partial \partial M} \tau_j$
$-\ln \langle \psi \psi \rangle$	$-\ln \text{tTr} \prod_j \hat{T}(j)$	Free energy

$t' \equiv \frac{1}{2} \ln \coth t$ is obtained via a Kramers-Wannier relation [68]. An immediate consequence of this factorization is that the phase diagram in Fig. 1 is controlled by two independent QPTs, tuned by h and t , respectively. The physical origin is that the m loops and the monopoles have trivial mutual statistics and can thus condense simultaneously. The classical TNs for ϵ_g and ϵ_p can both be equivalently generated, through cube-vertex duality, by a rank-6 tensor (Fig. 1, top right) where the tensor bond takes the plaquette variable $W_\square = \prod_{l \in \square} s_l$ or $W'_\square = \prod_{j \in \square} \tau_j$. To contract the TNs $\langle \psi | \psi \rangle$, we employ the variational infinite projected-entangled-paired-state (iPEPS) method to get the dominant boundary fixed point [69–74] (see SM). As in a general PEPS, the virtual variables serve as the entanglement degrees of freedom that are responsible for stretching out the long range entanglement [42,44,45,48,51]. This allows us to set up a dictionary between the quantum correlation and the classical correlations as in Table I. We elucidate the nature of the two QPTs in the following.

m-loop condensation.—This QPT is captured by the classical vector gauge model. A classical Wilson loop around an arbitrary membrane M excites an m -loop excitation above the ground state, which we denote as $|\prod_{p \in \partial M} m_p\rangle$. Consequently, the condensate fraction of m loops can be measured by its overlap with the ground state

$$\left\langle \psi \left| \prod_{p \in \partial M} m_p \right. \right\rangle = \left\langle \prod_{p \in \partial M} s_p \right\rangle = \left\langle \prod_{\square \in M} W_\square \right\rangle \equiv e^{-|M|/\xi_m^2}, \quad (6)$$

where $|M|$ denotes the area of M , and ξ_m defines the m -loop condensation length scale beyond which larger loops are orthogonal to the ground state. In the TN representation it is a membrane correlation written as a product of W_\square . An X operator to the virtual variable violates the local Gauss law and creates an e particle, equivalent to a semi-infinite 't Hooft string in the classical gauge theory, measuring the deconfined charge amplitude $\langle e|e\rangle$. Using Wegner's Ising-gauge duality [75], $\langle e|e\rangle$ is mapped to the dual Ising order parameter, and the critical point $h_c \approx 0.7614$ can be

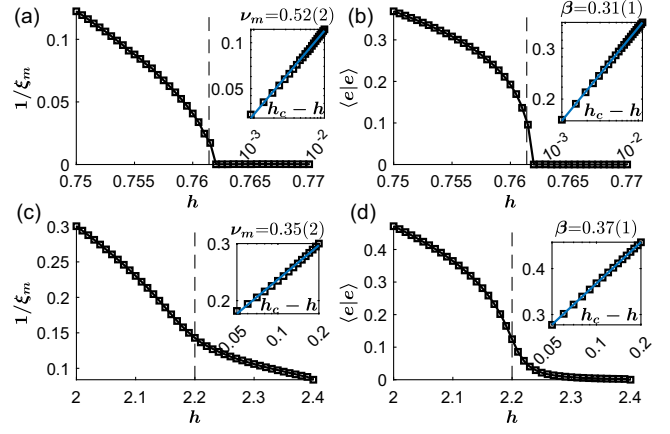


FIG. 2. QPT of m -loop condensation in the \mathbb{Z}_N model for (a),(b) $N = 2$ and (c),(d) $N = 5$. (a),(c) Inverse of the m -loop condensation length scale. (b),(d) Deconfined charge amplitude. Insets fit the critical exponents $\xi_m \propto |h_c - h|^{-\nu_m}$ and $\langle e|e\rangle \propto |h_c - h|^\beta$. Data are computed by iPEPS of bond dimension ($D = 3, \chi = 72$) for $N = 2$ and ($D = 2, \chi = 80$) for $N = 5$. Dashed vertical line denotes the critical point $h_c \approx 0.7614$ for $N = 2$ and $h_c \approx 2.2$ for $N = 5$.

deduced from the known 3D Ising critical temperature $2/\ln \coth h_c \approx 4.5115$ [76]. In Figs. 2(a) and 2(b) our iPEPS calculation shows that the loop condensation length scale ξ_m is finite if $h < h_c$ and diverges for $h \geq h_c$; near the Ising* critical point it obeys a scaling law with exponent $\nu_m = 0.52(2)$. The critical exponent β for the deconfined charge amplitude is also close to the Ising order parameter exponent 0.3295 [76]. Thus the divergence of the m -loop fluctuation length and the vanishing of the deconfined boson charge amplitude signal a continuous phase transition from the 2D TCs into the XC in the Ising* universality class [77].

Fracton confinement.—This QPT is described by the classical plaquette model. The model is invariant under planar subsystem Ising symmetries, which interpolate between the global and the local gauge symmetry [65–67,78] and are spontaneously broken across a first-order transition [68,79] at $t_c \simeq 0.66$. For an arbitrary membrane M , the probability amplitude for finding fractons at its corners (denoted by $\partial \partial M$) is measured by the wave function norm

$$\| \prod_{j \in \partial \partial M} f_j \|^2 = \left\langle \prod_{j \in \partial \partial M} \tau_j \right\rangle = \left\langle \prod_{\square \in M} W'_\square \right\rangle \equiv e^{-|M|/\xi_f^2}, \quad (7)$$

where f_j denotes the fracton, and ξ_f defines the fracton confining length scale, beyond which the fracton amplitude decays exponentially. $1/\xi_f^2$ is analogous to the string tension in the quark confinement [80]. Moreover, an X operator to the virtual variable violates the magnetic Gauss

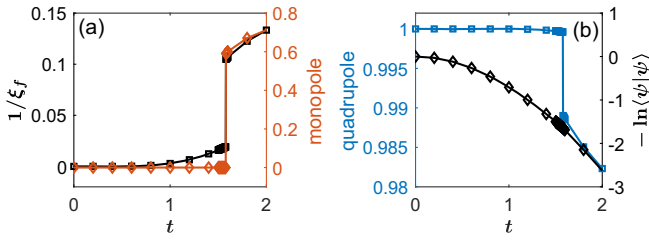


FIG. 3. Fracton confinement transition in the \mathbb{Z}_N model for $N = 24$. $t_c \approx 1.5788(13)$. (a) Left axis: inverse fracton-confinement lengthscale; right axis: monopole condensate fraction. (b) Left axis: fracton quadrupole amplitude; right axis: logarithm of the wave function norm mapped to the classical free energy density. Data are computed with iPEPS with bond dimension $D = 2$, $\chi = 24$.

law locally and creates a vector monopole excitation [57], whose expectation value measures the monopole condensate. An individual Z operator in the TN evaluates the classical plaquette operator W_{\square}^z , which corresponds to the probability of a fracton quadrupole around an elementary plaquette $\|\prod_{j \in \square} f_j\|^2$, which is a composite particle freely mobile in all directions. As shown in Fig. 3 and the SM, our iPEPS calculations indeed confirm the first-order transition across which the fracton confining length jumps from a large value for $t < t_c$ to a finite value when $t > t_c$, accompanied by a jump of the monopole condensate $\langle \psi | \text{monopole} \rangle$ from approximately zero to a finite value. The fracton quadrupole amplitude and the second Rényi entropy coefficient also exhibit a jump from approximately 1 to a finite value, and the effective free energy density as a generating function shows a clearly visible kink [81]. For $t < t_c$ the wave function with isolated fracton excitations and the degenerate ground states on a torus [9,12] are renormalizable and well defined. For $t > t_c$, the state with fractons separated at large distances has exponentially vanishing norm and is thus unrenormalizable, which means the fracton excitations as well as the topological degeneracy are gone in the thermodynamic limit—a hallmark for the breakdown of topological order. While $\langle \psi | \psi \rangle$ is interpreted as a partition function, from $\|\prod_{j \in \partial M} f_j\|^2 \propto e^{-F(M)}$ one may define a dimensionless free energy $F(M) = |M|/\xi_f^2$ which captures the energetics of a set of fracton excitations lying at the corners of M . $F(M)$ reflects the underlying entanglement structure of the ground state wave function [44,45,51], reminiscent of the fact that the dimensionless entanglement Hamiltonian from a pure ground state can also capture the low energy behavior of a true physical boundary [82–84].

\mathbb{Z}_N generalization.—All of the above can be generalized to the \mathbb{Z}_N gauge group, which interpolates between \mathbb{Z}_2 and the compact $U(1)$ gauge group. Importantly, the factorization (4) still holds and gives rise to a \mathbb{Z}_N lattice vector gauge model and a \mathbb{Z}_N generalization for the plaquette Ising model with planar \mathbb{Z}_N subsystem symmetries [57]. The \mathbb{Z}_N

vector gauge model [85,86] on a cubic lattice has been studied by using Kramers-Wannier duality to map it onto classical clock spin models exhibiting a single [87] transition depending on N : for $N \geq 5$ it is believed to undergo a continuous phase transition in the 3D XY universality class [85,86,88]. In our context, this implies that the m -loop condensation transition of our phase diagram in Fig. 1 persists in the generic \mathbb{Z}_N scenario (except for $N = 3$ where the transition at h_c becomes first order). Our iPEPS calculation for the \mathbb{Z}_5 case in Figs. 2(c) and 2(d) shows that the m -loop condensation length and the deconfined charge order parameter indeed approximately follow the conjectured scaling of the 3D XY universality class [89]. For the fracton confinement transition, on the other hand, our iPEPS calculations for the plaquette clock model with finite $N = 2, 3, \dots, 15, 16, 24$ indicate first-order transitions with finite jumps similar to the \mathbb{Z}_2 scenario (see Fig. 3 and SM), which however become notably weaker with increasing N .

$N \rightarrow \infty$ limit.—Of particular interest thus is the asymptotic limit in which \mathbb{Z}_N approaches the compact $U(1)$ gauge group. For the vector gauge model, Monte Carlo simulations [85,86] found that $h_c \propto N^2$, consistent with the absence of a deconfined $U(1)$ vector gauge phase in 3D [90]. For the plaquette model, we however find that the critical point converges to a finite value $t_c \rightarrow 1.58$ (Fig. 4). The inverse fracton confining length $1/\xi_f$ decreases $\propto 1/N$ (for t_c^+), and the transition jump of the quadrupole amplitude vanishes $\propto 1/N^2$. These numerical observations

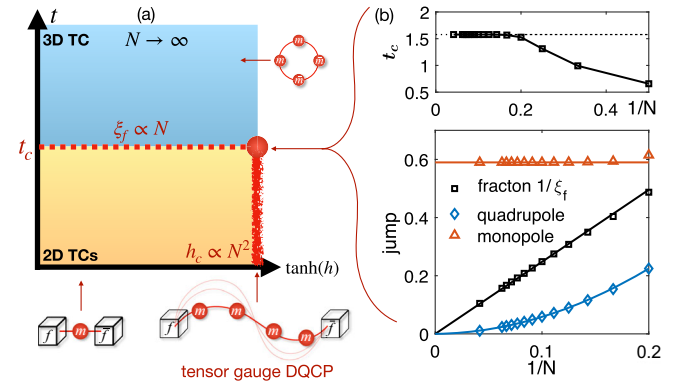


FIG. 4. Large- N limit. (a) Schematic phase diagram. The XC fracton phase shrinks to a quantum critical line at $\tanh(h_c) = 1$, on which deconfined fractons are glued by critical fluctuating m strings. h perturbation drives a partial confinement that binds fractons into a fracton dipole, adiabatically connected to the m particle in 2D TCs. $t > t_c$ drives complete confinement that leaves no deconfined fracton dipoles. (b) N -scaling for the first-order QPTs of \mathbb{Z}_N plaquette model: t_c converges to $t_c \approx 1.5775(25)$. The jump of the monopole condensate fraction remains finite and largely independent of N . The fracton confining length ξ_f for t_c^+ is proportional to N . The jump of fracton quadrupole amplitude vanishes like $1/N^2$. Data are computed with bond dimension $D = 2$ for $N = 2, \dots, 15, 16, 24$.

indicate that the deconfined $\mathbb{Z}_{N \rightarrow \infty}$ XC fracton phase shrinks to a critical line ($h_c \propto N^2$, $t \leq t_c$) in the asymptotic limit.

What is the nature of this critical line? The asymptotic limit can be described by the un-Higgsed $U(1)$ hollow tensor gauge theory studied in Refs. [20,22,24], where the electric field tensor is purely off diagonal so as to enhance the dipole conservation to subsystem charge conservation as an organizing principle [57]. Also, the classical plaquette model that our wave function is mapped onto, is equivalent to the classical field theory predicted for the Rokhsar-Kivelson point [20]. Such a 3D quantum tensor gauge theory is known to be generally unstable against monopole proliferation [20], which gaps out a deconfined Coulomb phase, analogous to the instability of a 2D quantum $U(1)$ vector gauge theory [90]. Nevertheless, it does not rule out the possibility that the deconfined gauge theory can emerge at a critical point, dubbed deconfined quantum critical point (DQCP) [91]. What we find here is a tensor gauge generalization of the vector gauge DQCP wave function [48], as the un-Higgsed fracton phase shrinks to a line of critical points decorated with critical fluctuating m strings that glue pairs of fractons (Fig. 4). As a consequence, the h perturbation is relevant (in the renormalization group sense) and confines two fractons into a fracton dipole. The fracton dipole is adiabatically connected to the deconfined m particle in the 2D TCs phase, signalling a partial confinement from the fracton state. On the other hand, sufficiently strong $t > t_c$ leads to monopole proliferation and confines not only the fractons but also the fracton dipoles. Notice that the adjacent phases of our DQCP do not exhibit spontaneous symmetry breaking but rather distinct topological orders. It remains to be understood why the jump of the monopole condensation order across t_c extrapolates to a finite value, which is mapped to the nonlocal symmetry twist defect in the classical model.

Outlook.—The two phase transition lines cross at a peculiar multicritical point that can serve as a parent critical state, upon which any perturbations are relevant and flow to all four possible topologically distinct states. It is straightforward to generalize the isotropic deformation to anisotropic deformation, covering a richer variety of anisotropic subdimensional criticalities in Refs. [34,38,39]. Our approach, by deforming an exact tensor-network state and mapping to a tunable and computable classical statistical model, can be further extended to type II fracton orders as fractal condensates [7,8], and twisted fracton topological order [92]. The wave function–deformed QPT of our study is particularly suitable for realization in programmable quantum simulators [4,5,93], where the application of a local nonunitary circuit can directly deform the wave function. Our 3D tensor network wave function also serves as a natural variational ansatz for Hamiltonian deformations, which we leave to future work.

We acknowledge partial funding from the Deutsche Forschungsgemeinschaft (DFG, German Research Foundation)—project Grant No. 277146847—through CRC network SFB/TRR 183 (projects A03, A04, B01). P. Y. was supported by NSFC Grant No. 12074438, Guangdong Basic and Applied Basic Research Foundation under Grant No. 2020B1515120100, and the Open Project of Guangdong Provincial Key Laboratory of Magnetoelectric Physics and Devices under Grant No. 2022B1212010008. J.-Y.C. acknowledges support from Sun Yat-sen University through a startup grant. The numerical simulations were performed on the CHEOPS cluster at the RRZK Cologne and on the JUWELS cluster at the Forschungszentrum Jülich using NLOpt package [94].

*gzhu@uni-koeln.de

†chenjy3@mail.sysu.edu.cn

‡yepeng5@mail.sysu.edu.cn

§trebst@thp.uni-koeln.de

- [1] X.-G. Wen, Colloquium: Zoo of quantum-topological phases of matter, *Rev. Mod. Phys.* **89**, 041004 (2017).
- [2] C. Nayak, S. H. Simon, A. Stern, M. Freedman, and S. Das Sarma, Non-Abelian anyons and topological quantum computation, *Rev. Mod. Phys.* **80**, 1083 (2008).
- [3] A. Kitaev, Fault-tolerant quantum computation by anyons, *Ann. Phys. (Amsterdam)* **303**, 2 (2003).
- [4] K. J. Satzinger *et al.*, Realizing topologically ordered states on a quantum processor, *Science* **374**, 1237 (2021).
- [5] G. Semeghini, H. Levine, A. Keesling, S. Ebadi, T. T. Wang, D. Bluvstein, R. Verresen, H. Pichler, M. Kalinowski, R. Samajdar, A. Omran, S. Sachdev, A. Vishwanath, M. Greiner, V. Vuletić, and M. D. Lukin, Probing topological spin liquids on a programmable quantum simulator, *Science* **374**, 1242 (2021).
- [6] C. Chamon, Quantum Glassiness in Strongly Correlated Clean Systems: An Example of Topological Overprotection, *Phys. Rev. Lett.* **94**, 040402 (2005).
- [7] J. Haah, Local stabilizer codes in three dimensions without string logical operators, *Phys. Rev. A* **83**, 042330 (2011).
- [8] B. Yoshida, Exotic topological order in fractal spin liquids, *Phys. Rev. B* **88**, 125122 (2013).
- [9] S. Vijay, J. Haah, and L. Fu, Fracton topological order, generalized lattice gauge theory, and duality, *Phys. Rev. B* **94**, 235157 (2016).
- [10] R. M. Nandkishore and M. Hermele, Fractons, *Annu. Rev. Condens. Matter Phys.* **10**, 295 (2019).
- [11] M. Pretko, X. Chen, and Y. You, Fracton phases of matter, *Int. J. Mod. Phys. A* **35**, 2030003 (2020).
- [12] H. Ma, E. Lake, X. Chen, and M. Hermele, Fracton topological order via coupled layers, *Phys. Rev. B* **95**, 245126 (2017).
- [13] S. Vijay, Isotropic layer construction and phase diagram for fracton topological phases, [arXiv:1701.00762](https://arxiv.org/abs/1701.00762).
- [14] W. Shirley, K. Slagle, Z. Wang, and X. Chen, Fracton Models on General Three-Dimensional Manifolds, *Phys. Rev. X* **8**, 031051 (2018).

- [15] X. Ma, W. Shirley, M. Cheng, M. Levin, J. McGreevy, and X. Chen, Fractonic order in infinite-component Chern-Simons gauge theories *Phys. Rev. B* **105**, 195124 (2022).
- [16] D. Aasen, D. Bulmash, A. Prem, K. Slagle, and D.J. Williamson, Topological defect networks for fractons of all types, *Phys. Rev. Res.* **2**, 043165 (2020).
- [17] K. Slagle, Foliated Quantum Field Theory of Fracton Order, *Phys. Rev. Lett.* **126**, 101603 (2021).
- [18] M.-Y. Li and P. Ye, Fracton physics of spatially extended excitations, *Phys. Rev. B* **101**, 245134 (2020).
- [19] M.-Y. Li and P. Ye, Fracton physics of spatially extended excitations. II. Polynomial ground state degeneracy of exactly solvable models, *Phys. Rev. B* **104**, 235127 (2021).
- [20] C. Xu and C. Wu, Resonating plaquette phases in SU(4) Heisenberg antiferromagnet, *Phys. Rev. B* **77**, 134449 (2008).
- [21] M. Pretko, Subdimensional particle structure of higher rank $U(1)$ spin liquids, *Phys. Rev. B* **95**, 115139 (2017).
- [22] H. Ma, M. Hermele, and X. Chen, Fracton topological order from the Higgs and partial-confinement mechanisms of rank-two gauge theory, *Phys. Rev. B* **98**, 035111 (2018).
- [23] D. Bulmash and M. Barkeshli, Higgs mechanism in higher-rank symmetric $U(1)$ gauge theories, *Phys. Rev. B* **97**, 235112 (2018).
- [24] N. Seiberg and S.-H. Shao, Exotic \mathbb{Z}_N symmetries, duality, and fractons in $3+1$ -dimensional quantum field theory, *SciPost Phys.* **10**, 3 (2021).
- [25] M. Pretko, The fracton gauge principle, *Phys. Rev. B* **98**, 115134 (2018).
- [26] A. Gromov, Towards Classification of Fracton Phases: The Multipole Algebra, *Phys. Rev. X* **9**, 031035 (2019).
- [27] N. Seiberg, Field theories with a vector global symmetry, *SciPost Phys.* **8**, 050 (2020).
- [28] J.-K. Yuan, S. A. Chen, and P. Ye, Fractonic superfluids, *Phys. Rev. Res.* **2**, 023267 (2020).
- [29] S. A. Chen, J.-K. Yuan, and P. Ye, Fractonic superfluids. II. Condensing subdimensional particles, *Phys. Rev. Res.* **3**, 013226 (2021).
- [30] H. Li and P. Ye, Renormalization group analysis on emergence of higher rank symmetry and higher moment conservation, *Phys. Rev. Res.* **3**, 043176 (2021).
- [31] J.-K. Yuan, S. A. Chen, and P. Ye, Hierarchical proliferation of higher-rank symmetry defects in fractonic superfluids, *Phys. Rev. B* **107**, 205134 (2023).
- [32] C. Stahl, E. Lake, and R. Nandkishore, Spontaneous breaking of multipole symmetries, *Phys. Rev. B* **105**, 155107 (2022).
- [33] S. A. Chen, and P. Ye, Exploring Spontaneous Symmetry Breaking through Fractonic Superfluids, [arXiv:2305.00941](https://arxiv.org/abs/2305.00941).
- [34] K. Slagle and Y. B. Kim, Fracton topological order from nearest-neighbor two-spin interactions and dualities, *Phys. Rev. B* **96**, 165106 (2017).
- [35] T. Devakul, S. A. Parameswaran, and S. L. Sondhi, Correlation function diagnostics for type-I fracton phases, *Phys. Rev. B* **97**, 041110(R) (2018).
- [36] M. Mühlhauser, M. R. Walther, D. A. Reiss, and K. P. Schmidt, Quantum robustness of fracton phases, *Phys. Rev. B* **101**, 054426 (2020).
- [37] T. F. J. Poon and X.-J. Liu, Quantum phase transition of fracton topological orders, *Phys. Rev. Res.* **3**, 043114 (2021).
- [38] E. Lake and M. Hermele, Subdimensional criticality: Condensation of lineons and planons in the X-cube model, *Phys. Rev. B* **104**, 165121 (2021).
- [39] B. C. Rayhaun and D. J. Williamson, Higher-form subsystem symmetry breaking: Subdimensional criticality and fracton phase transitions, [arXiv:2112.12735](https://arxiv.org/abs/2112.12735).
- [40] M. Mühlhauser, K. P. Schmidt, J. Vidal, and M. R. Walther, Competing topological orders in three dimensions, *SciPost Phys.* **12**, 69 (2022).
- [41] E. Ardonne, P. Fendley, and E. Fradkin, Topological order and conformal quantum critical points, *Ann. Phys. (Amsterdam)* **310**, 493 (2004).
- [42] J. I. Cirac, D. Pérez-García, N. Schuch, and F. Verstraete, Matrix product states and projected entangled pair states: Concepts, symmetries, theorems, *Rev. Mod. Phys.* **93**, 045003 (2021).
- [43] C. Castelnovo, S. Trebst, and M. Troyer, Topological Order and Quantum Criticality, in *Understanding Quantum Phase Transitions* (Taylor & Francis, London, 2010), pp. 169–192.
- [44] N. Schuch, D. Poilblanc, J. I. Cirac, and D. Pérez-García, Topological Order in the Projected Entangled-Pair States Formalism: Transfer Operator and Boundary Hamiltonians, *Phys. Rev. Lett.* **111**, 090501 (2013).
- [45] J. Haegeman, V. Zauner, N. Schuch, and F. Verstraete, Shadows of anyons and the entanglement structure of topological phases, *Nat. Commun.* **6**, 8284 (2015).
- [46] K. Duivenvoorden, M. Iqbal, J. Haegeman, F. Verstraete, and N. Schuch, Entanglement phases as holographic duals of anyon condensates, *Phys. Rev. B* **95**, 235119 (2017).
- [47] J.-Y. Chen and D. Poilblanc, Topological \mathbb{Z}_2 resonating-valence-bond spin liquid on the square lattice, *Phys. Rev. B* **97**, 161107(R) (2018).
- [48] G.-Y. Zhu and G.-M. Zhang, Gapless Coulomb State Emerging from a Self-Dual Topological Tensor-Network State, *Phys. Rev. Lett.* **122**, 176401 (2019).
- [49] W.-T. Xu, Q. Zhang, and G.-M. Zhang, Tensor Network Approach to Phase Transitions of a Non-Abelian Topological Phase, *Phys. Rev. Lett.* **124**, 130603 (2020).
- [50] Q. Zhang, W.-T. Xu, Z.-Q. Wang, and G.-M. Zhang, Non-Hermitian effects of the intrinsic signs in topologically ordered wavefunctions, *Commun. Phys.* **3**, 209 (2020).
- [51] M. Iqbal and N. Schuch, Entanglement Order Parameters and Critical Behavior for Topological Phase Transitions and Beyond, *Phys. Rev. X* **11**, 041014 (2021).
- [52] D. Poilblanc and M. Mambrini, Quantum critical phase with infinite projected entangled paired states, *Phys. Rev. B* **96**, 014414 (2017).
- [53] P. Corboz, P. Czarnik, G. Kapteijns, and L. Tagliacozzo, Finite Correlation Length Scaling with Infinite Projected Entangled-Pair States, *Phys. Rev. X* **8**, 031031 (2018).
- [54] M. Rader and A. M. Läuchli, Finite Correlation Length Scaling in Lorentz-Invariant Gapless iPEPS Wave Functions, *Phys. Rev. X* **8**, 031030 (2018).
- [55] J.-Y. Chen, S. Capponi, A. Wietek, M. Mambrini, N. Schuch, and D. Poilblanc, $SU(3)_1$ Chiral Spin Liquid on the Square Lattice: A View from Symmetric Projected Entangled Pair States, *Phys. Rev. Lett.* **125**, 017201 (2020).

- [56] N. Tantivasadakarn, W. Ji, and S. Vijay, Hybrid fracton phases: Parent orders for liquid and nonliquid quantum phases, *Phys. Rev. B* **103**, 245136 (2021).
- [57] See Supplemental Material at <http://link.aps.org/supplemental/10.1103/PhysRevLett.130.216704> for numerical phase diagrams of the \mathbb{Z}_N plaquette model; frustration-free Rokhsar-Kivelson Hamiltonian; \mathbb{Z}_N generalization of coupled toric code layers; quantum classical mapping; X cube model and its tensor-network wave functions; a map from \mathbb{Z}_N X-cube model to \mathbb{Z}_N tensor-gauge theory; boundary fixed point iPEPS method; supplemental data for \mathbb{Z}_N toric code QPT; supplemental data for \mathbb{Z}_N X cube QPT; fracton dipole condensation in pure X cube; and comparison with previous studies into the fracton QPT.
- [58] A. Hamma, P. Zanardi, and X.-G. Wen, String and membrane condensation on three-dimensional lattices, *Phys. Rev. B* **72**, 035307 (2005).
- [59] Note that we can construct an exact Rokhsar-Kivelson type, frustration free Hamiltonian [41,60] that stabilizes $|\psi(t, h)\rangle$ as its ground state $H_{\text{RK}} = H_0 + \sum_{\square} \hat{V}_{\square} + \sum_{+} \hat{V}'_{+}$, with H_0 being the Hamiltonian of stacked uncoupled 2D TCs, while $\hat{V}_{\square} = e^{-h \sum_{i \in \square} \mu_i^z}$ and $\hat{V}'_{+} = e^{-t \sum_{i \in +} \sigma_i^x}$. A detailed proof is given in the SM.
- [60] C.L. Henley, From classical to quantum dynamics at Rokhsar-Kivelson points, *J. Phys. Condens. Matter* **16**, S891 (2004).
- [61] H. He, Y. Zheng, B.A. Bernevig, and N. Regnault, Entanglement entropy from tensor network states for stabilizer codes, *Phys. Rev. B* **97**, 125102 (2018).
- [62] D. J. Williamson, C. Delcamp, F. Verstraete, and N. Schuch, On the stability of topological order in tensor network states, *Phys. Rev. B* **104**, 235151 (2021).
- [63] S. V. Isakov, P. Fendley, A. W. W. Ludwig, S. Trebst, and M. Troyer, Dynamics at and near conformal quantum critical points, *Phys. Rev. B* **83**, 125114 (2011).
- [64] J. B. Kogut, An introduction to lattice gauge theory and spin systems, *Rev. Mod. Phys.* **51**, 659 (1979).
- [65] G. Savvidy and F. Wegner, Geometrical string and spin systems, *Nucl. Phys.* **B413**, 605 (1994).
- [66] R. Pietig and F. Wegner, Low temperature expansion of the gonihedric Ising model, *Nucl. Phys.* **B525**, 549 (1998).
- [67] C. Xu and J. E. Moore, Strong-Weak Coupling Self-Duality in the Two-Dimensional Quantum Phase Transition of $p + ip$ Superconducting Arrays, *Phys. Rev. Lett.* **93**, 047003 (2004).
- [68] M. Mueller, W. Janke, and D. A. Johnston, Nonstandard Finite-Size Scaling at First-Order Phase Transitions, *Phys. Rev. Lett.* **112**, 200601 (2014).
- [69] L. Vanderstraeten, J. Haegeman, P. Corboz, and F. Verstraete, Gradient methods for variational optimization of projected entangled-pair states, *Phys. Rev. B* **94**, 155123 (2016).
- [70] P. Corboz, Variational optimization with infinite projected entangled-pair states, *Phys. Rev. B* **94**, 035133 (2016).
- [71] L. Vanderstraeten, B. Vanhecke, and F. Verstraete, Residual entropies for three-dimensional frustrated spin systems with tensor networks, *Phys. Rev. E* **98**, 042145 (2018).
- [72] H.-J. Liao, J.-G. Liu, L. Wang, and T. Xiang, Differentiable Programming Tensor Networks, *Phys. Rev. X* **9**, 031041 (2019).
- [73] P. C. G. Vlaar and P. Corboz, Simulation of three-dimensional quantum systems with projected entangled-pair states, *Phys. Rev. B* **103**, 205137 (2021).
- [74] J. Nocedal and S. J. Wright, *Numerical Optimization*, 2nd ed. (Springer, New York, 2006).
- [75] F. J. Wegner, Duality in generalized Ising models and phase transitions without local order parameters, *J. Math. Phys.* (N.Y.) **12**, 2259 (1971).
- [76] Z. Y. Xie, J. Chen, M. P. Qin, J. W. Zhu, L. P. Yang, and T. Xiang, Coarse-graining renormalization by higher-order singular value decomposition, *Phys. Rev. B* **86**, 045139 (2012).
- [77] S. Trebst, P. Werner, M. Troyer, K. Shtengel, and C. Nayak, Breakdown of a Topological Phase: Quantum Phase Transition in a Loop Gas Model with Tension, *Phys. Rev. Lett.* **98**, 070602 (2007).
- [78] C. Xu and J. Moore, Reduction of effective dimensionality in lattice models of superconducting arrays and frustrated magnets, *Nucl. Phys.* **B716**, 487 (2005).
- [79] D. A. Johnston, M. Mueller, and W. Janke, Plaquette Ising models, degeneracy and scaling, *Eur. Phys. J. Spec. Top.* **226**, 749 (2017).
- [80] M. Creutz, Monte Carlo study of quantized SU(2) gauge theory, *Phys. Rev. D* **21**, 2308 (1980).
- [81] We note that the nonzero $1/\xi_f$ at $t < t_c$ is due to the finite bond dimension effect of the iPEPS ansatz which cannot truly capture infinite correlation length, and ξ_f shall grow larger with larger bond dimension (see SM).
- [82] H. Li and F. D. M. Haldane, Entanglement Spectrum as a Generalization of Entanglement Entropy: Identification of Topological Order in Non-Abelian Fractional Quantum Hall Effect States, *Phys. Rev. Lett.* **101**, 010504 (2008).
- [83] J. I. Cirac, D. Poilblanc, N. Schuch, and F. Verstraete, Entanglement spectrum and boundary theories with projected entangled-pair states, *Phys. Rev. B* **83**, 245134 (2011).
- [84] X.-L. Qi, H. Katsura, and A. W. W. Ludwig, General Relationship between the Entanglement Spectrum and the Edge State Spectrum of Topological Quantum States, *Phys. Rev. Lett.* **108**, 196402 (2012).
- [85] G. Bhanot and M. Creutz, Phase diagram of $Z(N)$ and $U(1)$ gauge theories in three dimensions, *Phys. Rev. D* **21**, 2892 (1980).
- [86] O. Borisenko, V. Chelnokov, G. Cortese, M. Gravina, A. Papa, and I. Surzhikov, Critical behavior of 3D $Z(N)$ lattice gauge theories at zero temperature, *Nucl. Phys.* **B879**, 80 (2014).
- [87] The clock anisotropy is dangerously irrelevant at the 3D XY critical point [88], which indicates the absence of a stable intermediate Coulomb phase in the thermodynamic limit, and thus only a single transition.
- [88] M. Oshikawa, Ordered phase and scaling in Z_n models and the three-state antiferromagnetic Potts model in three dimensions, *Phys. Rev. B* **61**, 3430 (2000).
- [89] M. Campostrini, M. Hasenbusch, A. Pelissetto, P. Rossi, and E. Vicari, Critical behavior of the three-dimensional XY universality class, *Phys. Rev. B* **63**, 214503 (2001).

- [90] A. Polyakov, Quark confinement and topology of gauge theories, *Nucl. Phys.* **B120**, 429 (1977).
- [91] T. Senthil, A. Vishwanath, L. Balents, S. Sachdev, and M. P. A. Fisher, Deconfined quantum critical points, *Science* **303**, 1490 (2004).
- [92] H. Song, A. Prem, S.-J. Huang, and M. A. Martin-Delgado, Twisted fracton models in three dimensions, *Phys. Rev. B* **99**, 155118 (2019).
- [93] D. Bluvstein, H. Levine, G. Semeghini, T. T. Wang, S. Ebadi, M. Kalinowski, A. Keesling, N. Maskara, H. Pichler, M. Greiner, V. Vuletic, and M. D. Lukin, A quantum processor based on coherent transport of entangled atom arrays, *Nature (London)* **604**, 451 (2022).
- [94] S. G. Johnson, The nLopt nonlinear-optimization package, <http://github.com/stevengj/nlopt>.